

Background climate conditions regulated the photosynthetic response of Amazon forests to the 2015/2016 El Niño-Southern Oscillation event

Max Fancourt ^{1,3}✉, Guy Ziv ^{1,3}, Klaas Folkert Boersma^{2,4}, Julia Tavares^{1,4}, Yunxia Wang^{1,4} & David Galbraith ^{1,3}

Amazon forests have experienced multiple large-scale droughts in recent decades, which have increased tree mortality and reduced carbon sequestration. However, the extent to which drought sensitivity varies across Amazonian forests and its key controls remain poorly quantified. Here, we analyse satellite remotely-sensed Solar Induced Fluorescence anomalies to investigate responses in Amazon forest photosynthetic activity to the 2015–2016 El Niño–Southern Oscillation (ENSO) drought. Using multivariate regression analysis, we examine the relative importance of ENSO-associated climate anomalies, background climate and soil characteristics in controlling basin-wide forest photosynthetic activity differences. Our model explains 25% of forest photosynthetic response and indicates background climate and soil conditions had a greater influence than the climatic anomalies experienced. We find marked sensitivity differences across Amazonia, with North-Western forests being the most sensitive to precipitation anomalies, likely relating to variation in forest species composition and background water stress. Such factors should be considered in climate change impact simulations.

¹University of Leeds, Leeds, UK. ²Wageningen University, Wageningen, Netherlands. ³These authors contributed equally: Max Fancourt, David Galbraith, Guy Ziv. ⁴These authors jointly supervised this work: Klaas Folkert Boersma, Julia Tavares, Yunxia Wang. ✉email: max.fancourt@gmail.com

The tropical forests of Amazonia provide extensive ecosystem services both locally and globally¹ including unparalleled biodiversity provision^{2,3}, regulation of regional climate⁴ and substantial carbon storage⁵. The high and multi-dimensional nature of their value means that it is critical to better understand their ability to resist stressors and maintain the provision of these services. Extreme climatic anomalies are a major threat to the services provided by Amazon forests. In recent decades, Amazon forests have been exposed to a number of large climatic anomalies including in 2005⁶, 2010⁷, and 2015/16⁸. These droughts have resulted in losses of aboveground biomass due to widespread tree mortality^{7,9} and decreased Gross Primary Productivity (GPP)¹⁰.

Previous assessments of Amazonian droughts based on forest inventory plots have sought to quantify the impact on the basin-wide carbon sink^{7,9,11} but have not explicitly addressed the extent to which Amazon forests differ in their response to such climatic anomalies at sub-basin scales. The variance in response may be substantial as plot scale studies of plant hydraulic properties suggest that forest sensitivity to water stress can vary greatly even at a local level^{12,13}. However, scaling up plot-based responses to climatic anomalies in order to explore the implications across larger scales in Amazonia is difficult, because of the limited number of sampling sites that can be realistically be measured following an extreme climate anomaly.

Remotely sensed data allows for variation in the sensitivity of forest productivity to climatic anomalies to be more fully explored across space with the caveat that photosynthesis is not directly being measured, but instead inferred from spectral signatures. Remote sensing of solar-induced fluorescence (SIF) is a particularly powerful proxy of forest productivity and has been shown to strongly track GPP at seasonal timescales, including in tropical forests^{10,14}. SIF has been used previously to evaluate the effects of several large climatic anomalies, including the impacts of the 2015/2016 ENSO on tropical forests^{10,15,16}. Although these studies have highlighted the widespread negative SIF anomalies associated with the ENSO event across Amazonia, they involved no formal pixel-level analysis of SIF anomalies across space.

The response of forest productivity to extreme climatic anomalies is moderated by a wide range of factors which can be broadly classified into three groups: (i) the intensity of the climate anomaly itself, (ii) the background (long-term mean) climatology and (iii) soil characteristics. Forest plot studies have highlighted significant relationships between drought intensity based on precipitation anomalies and biomass losses following large drought events^{9,11}. Temperature anomalies have the potential to amplify these effects¹⁷. Background climate and soil characteristics can substantially modulate the impacts of anomalous climatic events. Forest sensitivity to water stress may be related to background climate as forests found in drier regions have been shown to be better adapted hydraulically to drought than those found in wetter environments¹⁸. Mean annual precipitation varies widely across Amazonian forests, as does the seasonality and interannual variability in rainfall, greatly affecting species composition¹⁹ and forest resilience to drought¹⁵. Soil properties can further strongly modulate responses to drought events²⁰. Soil texture exerts a strong control on water holding capacity and hydraulic conductivity²¹ while water table depth can greatly influence forest access to water, with forests on deeper water tables expected to be more at risk of water shortage during drought events compared to shallower water table areas¹². This relative vulnerability of deep water table forests is despite these forests containing more drought-tolerant species²², and is driven by the ability of shallow water table areas to buffer the negative effects of drought through the groundwater memory effect²². While it is clear that each of these variables plays a role in

determining Amazon forest response to climate, their relative importance in regulating response to natural climatic anomalies remains unclear.

In this study, we use a multivariate regression framework to explicitly evaluate the relative importance of ENSO-associated climate anomalies, soil characteristics and background climate variables as controls of Amazon forest photosynthetic anomalies during the drought associated with the 2015/16 ENSO. The 2015/16 ENSO event was associated with the most extreme drought and period of warming on record¹⁶ and thus offers an ideal case study in terms of the strength of signal-to-noise ratios. Using this methodology we found that background climate and soil conditions were more important controls on forest photosynthesis responses than the magnitude of the climate anomalies associated with the ENSO in explaining the variance in SIF anomalies. Our results reveal marked differences in sensitivity Amazonian regions response, with Northwestern Amazonian forests being the most and the Southwestern forests the least sensitive to precipitation anomalies. These differences in sensitivity likely relate to community species compositional differences across Amazonian forests, which vary greatly in the extent to which they are pre-adapted to water stress, and need to be accounted for in simulations of climate change impacts.

Results and discussion

Solar Induced Fluorescence during the 2015/2016 ENSO. To evaluate the impact of 2015/2016 ENSO on Amazon forest photosynthesis we computed standardised anomalies defined as:

$$\text{Standardised anomaly} = \frac{X_t - \bar{X}}{\sigma} \quad (1)$$

where X_t represents the mean SIF/climatic value during the October to December 2015 period, \bar{X} represents the mean and σ the standard deviation of the baseline period (October to December) between 2007 and 2014 (excluding 2015). In line with the findings of previous studies^{10,16,23}, retrievals based on SIFTERv2.0 show widespread negative SIF anomalies, across Amazonia. Indeed, 93% of forested pixels in our study domain exhibited negative SIF anomalies during October–December 2015, and mean pixel-level SIF over this time window was 1.03 standard deviations lower than baseline values. Moreover, anomalies during this time period (delineated by the vertical dashed lines in Fig. 1) are the most negative on record in all Amazonian regions except the Southwestern (SW) Amazon.

Climate anomalies during the 2015/2016 ENSO. Surprisingly, we find that ENSO-associated climate anomalies (anomalies in precipitation, temperature, and Maximum Cumulative Water Deficit (MCWD)) were very poor predictors of the observed variation in the mean standardised SIF anomaly for Oct-Dec 2015 (hereafter referred to as the standardised SIF anomaly) during the peak of the drought associated with the ENSO. Indeed, a linear model constructed exclusively with variables describing ENSO-associated climate anomalies explained only 2% of the regional variation in SIF anomalies (Table 1). This contrasts significantly with our final multivariate linear model, which models SIF anomaly as a function of soil characteristics and background climate variables in addition to ENSO-associated climate anomalies and which accounted for 25% of the variation in SIF anomaly (for full model see Supplementary Table 1). Given the relatively coarse scale at which this study is being conducted, and the fact that forest-scale ecological responses are typically noisy, the amount of variance explained by our final model is reasonable and comparable with that found in plot scale studies. For instance, the best model of Sullivan et al.²⁴ for woody

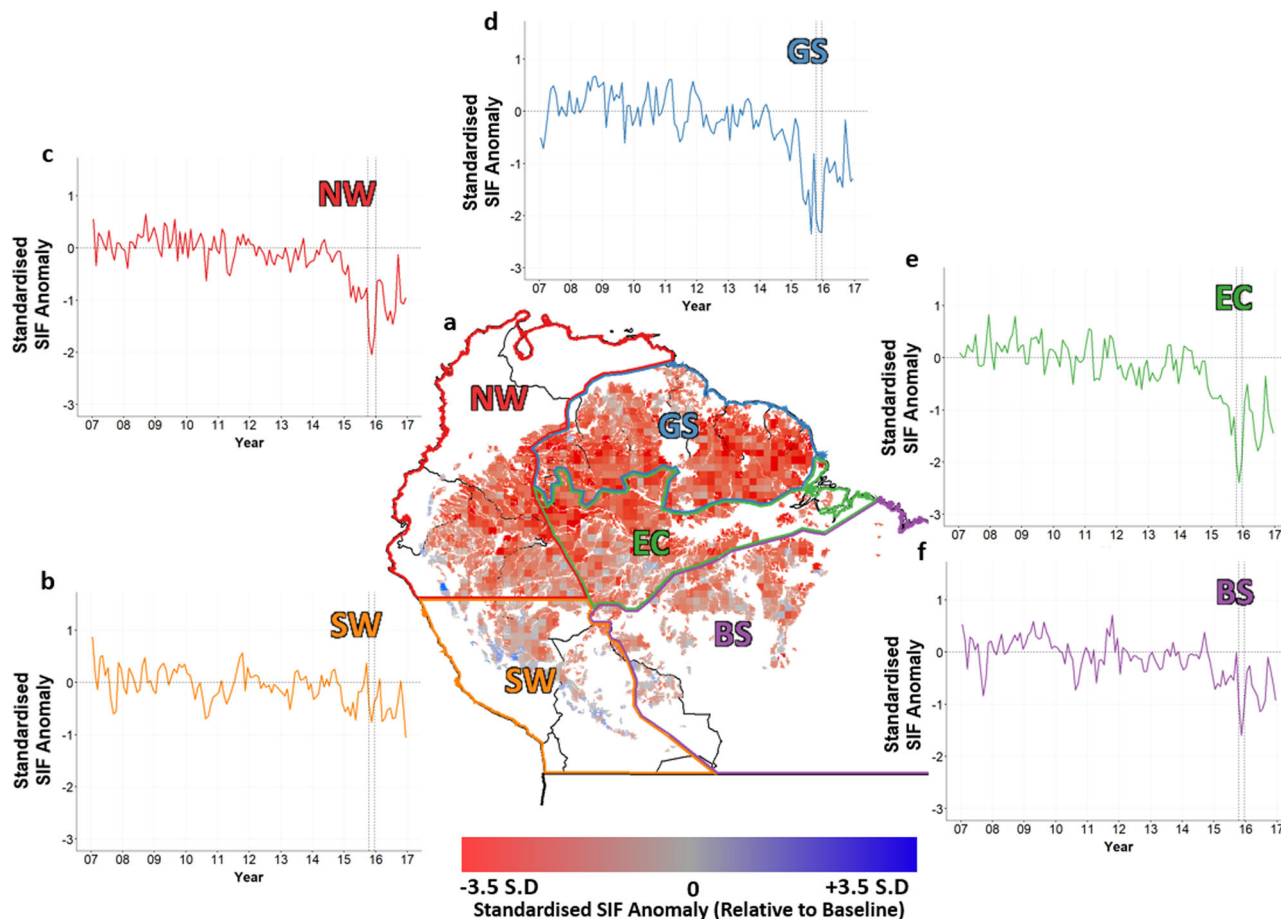


Fig. 1 Spatial distribution of Solar Induced Fluorescence Anomaly during the 2015/16 ENSO and temporal trends in SIF anomaly at a regional scale. **a** Spatial distribution of mean standardised SIF anomaly for October–December 2015. **b–f** Monthly Standardised Solar Induced Fluorescence (SIF) anomalies from January 2007 to December 2017. Results are split by geographical regions established by Feldpausch et al.⁴⁴. Vertical dashed lines signify the 2015 Oct–Nov–Dec period used in this study. **b** SW South West, **c** NW North West; **d** GS Guiana Shield, **e** EC East Central, **f** BS Brazilian Shield. Analysis is restricted to natural forests as defined by the Intact Forest data product⁴⁶. See methods for details.

Table 1 Proportion of variation explained by groups of predictor variables and the impact of their removal on the explanatory power of the final model.

ENSO-associated climate anomalies	Background climate	Soil characteristics	Adjusted R^2	Drop in R^2 compared to full model	Change in AIC compared to full model
✓	✓	✓	25%	-	-
✓	✓	✓	24%	1%	+28
✓	✓	✓	14%	11%	+270
✓	✓		19%	6%	+165
✓			2%	23%	+553
	✓		17%	8%	+215
		✓	12%	13%	+319

The final, full model is highlighted in bold. All values are rounded to nearest integer.

productivity (based on changes in diameter over time), explained 30% of the observed variation.

The relatively low importance of the ENSO-associated climate anomalies is further highlighted by the fact that removal of soil characteristics and background climate variables from this final model resulted in a far greater reduction in explanatory power as observed in change in adjusted R^2 , and in the increase in Aikake Information Criteria (AIC) than dropping variables denoting ENSO strength (Table 1). Of the three groups, the background climate variables were found to be particularly important, as its

removal resulted in a substantial lowering of R^2 from 0.25 to 0.14, and an increase in AIC of +270.

The role of soil characteristics and background climate variables in explaining photosynthetic response. The importance of soil characteristics and background climate variables on photosynthetic anomalies is further confirmed through the evaluation of the standardised regression coefficients of individual predictors in this final model which is summarised visually in Fig. 2. The

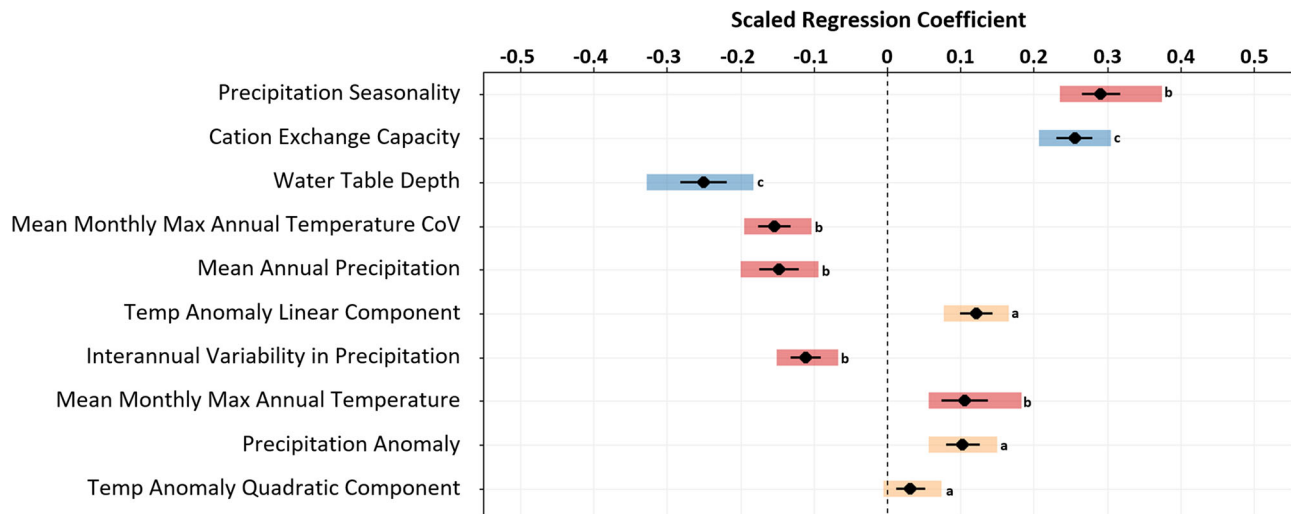


Fig. 2 Scaled and centred regression coefficients of final model variables. Scaled and centred regression coefficients for all variables found in the final model. Variables have been ranked by absolute magnitude of regression coefficient. Wings are standard errors and bars represent the 95% confidence intervals estimated via a bootstrapping analysis. Bars are coloured and numbered according to variable group: **a** yellow indicating ENSO-associated climate anomalies variables, **b** red denotes background climate variables and **c** blue represents soil characteristics.

sign and magnitude of the standardised regression coefficients in Fig. 2 describe the relationship between SIF Anomaly and the explanatory variable as part of the overall contribution of all variables towards the model prediction of SIF anomaly, all other variables being held constant. Positive coefficient values, for instance, indicate a positive relationship between explanatory variables and SIF Anomaly. Hence, a unit increase in the explanatory variable will contribute a positive amount to the SIF anomaly model prediction, all other variables being held constant. Applying this logic to our explanatory variables allows understanding of which traits contribute positively and negatively to SIF anomalies.

The five most important variables in the final model, ranked in order of descending importance based on the magnitudes of the standardised regression coefficients were: (1) rainfall seasonality, (2) cation exchange capacity, (3) water table depth, (4) variation in monthly max temperature, and (5) mean annual precipitation. Precipitation anomaly during the peak of the drought emerged as only the ninth most important explanatory variable. Overall, our results suggest that forests found in regions with high rainfall seasonality, high soil fertility, lower water table depth, and which have a higher monthly variation in max temperature and lower mean annual precipitation are more resistant to the drought associated with the ENSO than wetter, more aseasonal forests and forests on lower fertility soils and deeper water tables. However, we do not find evidence that forests exposed to higher interannual rainfall variability were more resistant to the drought, as has been inferred in previous studies based on examination of tree cover distributions¹⁵ nor do we find a significant role of soil texture in mediating photosynthetic response to this drought. (The spatial distribution of all predictor variables are shown in Supplementary Fig. 3).

The overarching importance of background climate, water table depth and soil fertility relative to ENSO-associated climate anomalies helps to explain the weak spatial structure in SIF anomalies observed (Fig. 1), despite substantial spatial variation in the ENSO-associated climatic anomalies (Supplementary Fig. 1). Amazonian forests vary greatly in background climate²⁵, soils²⁶ and water table depth²⁷ and these system properties translate into considerable differences across forests in sensitivity to this drought. Using SIF anomaly and climate anomaly data, we

calculated sensitivity (defined as standardised SIF anomaly/climate anomaly) of Amazon forest photosynthesis to precipitation and temperature anomalies at the pixel level (Fig. 3). Using this approach, we identified marked variation in sensitivity to climate in forests in different biogeographical regions. North-western (NW) Amazonia is the wettest and least seasonal region in Amazonia in terms of rainfall and temperature seasonality (Supplementary Fig. 3 for spatial variation) although variation in temperature seasonality is generally low across the entire study domain. Forests in the NW region were found to be the most sensitive to precipitation reduction being twice as sensitive as the Amazon-wide mean, and more than 12 times as sensitive as the least sensitive BS region. On the other hand, the forests of the Brazilian Shield (BS) which are the driest and most seasonal in the Basin were found to be least sensitive to precipitation reduction and were five times less sensitive than the Amazon-wide mean. The Guiana Shield (GS) region, simulated by many climate models to be the region most likely to be affected by future rainfall reduction²⁸ was found to be the third most sensitive to rainfall change during this drought after NW and EC Amazonia. Whereas there is clear evidence of different sensitivity to precipitation across Amazonian regions, differences in sensitivity to temperature are less obvious (Fig. 3), and might reflect the fact that spatial variation in temperature across Amazonia is much less marked than the spatial variation in precipitation.

The role of community species composition in determining variance in response. The effects of background climate, water table depth and soils on forest resistance to this drought, and droughts more generally, are ultimately mediated via tree species composition. Seasonal water stress has been found to exert a fundamental control on the biogeographical distributions of Amazonian tree species, with many species being restricted in range to the wetter regions of the Amazon¹⁹. Over more local scales, variation in water table depth can also strongly influence community species composition, with near complete species turnover observed in closely occurring forest plots on shallow water tables compared to those on deeper water tables²⁹. Such large differences in floristic composition along water availability axes are likely associated with differences in community-level

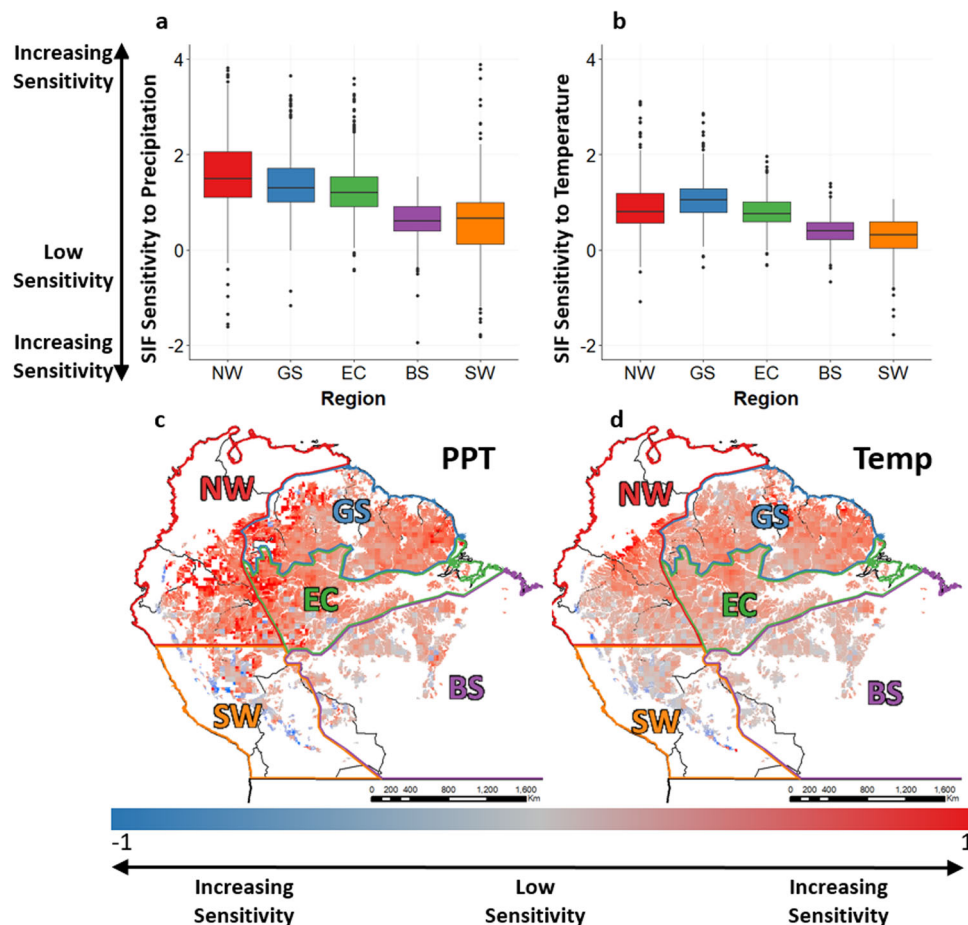


Fig. 3 Spatial distribution and regional averages of SIF sensitivity to temperature and precipitation anomalies. **a, b** Show precipitation (**a**) and temperature (**b**) regionally averaged sensitivities. SIF Sensitivity is calculated as $\text{Log}_{10}(\text{Standardised SIF Anomaly} / \text{Standardised PPT Anomaly})$ and $\text{Log}_{10}(\text{Standardised SIF Anomaly} / \text{Standardised Temp Anomaly})$ respectively. Box plot centre line, top, and bottom line represent the median, 75th, and 25th percentile, respectively. Upper and lower whiskers represent the largest and smallest value within 1.5 times the interquartile range above and below the 75th/25th percentile respectively. Results are split by geographical regions established by Feldpausch et al.⁴⁴. **c, d** Spatial distribution of SIF sensitivity to precipitation (**c**) and temperature (**d**). Sensitivity was calculated only for pixels that represented, negative precipitation, and positive temperature anomalies respectively. Temperature sensitivity has been inverted to aid in visual interpretation.

drought tolerance. It has been shown for example that species occurrence along hydro-topographic gradients in Central Amazonia is underpinned by differences in embolism resistance³⁰, as species occurring on water-limited plateau areas are considerably more embolism-resistant than those occurring in valley areas with more access to water³⁰. Community-level differences in hydraulic traits have been found to explain why a more seasonal Amazon forest experiencing a strong drought anomaly during the 2015/16 ENSO presented a similar canopy conductance response to a less seasonal forest experiencing a weaker climatic anomaly¹³. Our results raise the prospect that such a compensatory mechanism may have been in operation at a Basin-wide scale during the drought associated with the 2015/16 ENSO as forests that experienced less severe climatic anomalies but are less adapted to water stress experienced similar reductions in photosynthesis to forests that experienced more severe climatic anomalies but are more adapted to seasonal drought.

The positive relationship between cation exchange capacity and SIF anomaly may reflect differences in the life history strategies of species along fertility gradients. Amazon forests on fertile soils are generally more dynamic and more productive than those found on infertile soils²⁶. The functional attributes of tree species occurring on fertile soils, such as low leaf mass per area (LMA) and high foliar N and P content³¹ are indicative of species with

acquisitive (high resource acquisition rates and high growth that tend to do better in high resource habitats³²) rather than conservative life histories (geared towards high resource conservation, high-stress tolerance and high survival which tend to be more successful in lower resource habitats³²) and thus prioritising growth over survival. Forest communities consisting largely of acquisitive species would be more likely to maintain photosynthesis rates high under drought, despite increased risk of hydraulic cavitation, than communities consisting of more conservative species^{33,34}. Although the interaction between nutrient availability and drought impact has been largely unstudied in tropical forests, our results are consistent with analyses of temperate systems which found that more fertile soils enhanced resistance of tree growth to drought³⁵.

Our finding that Amazon forest response to ENSO-associated climatic anomalies is controlled more by the sensitivity of the forests and less by the intensity of the event has important implications. It suggests that insights derived from well-studied sites in Central and Eastern Amazonia e.g. Barros et al. 2015, and Rowland et al. 2015^{13,36} may not be readily generalisable to other regions of the Amazon, which may be more sensitive (e.g., NW Amazonia) or less sensitive (e.g. SW Amazonia) to reduced rainfall. Our results also highlight the pitfalls of assuming a universal sensitivity of Amazonian forests to drought in

ecosystem models. Most widely employed global vegetation models incorporate a very limited functional diversity across Amazonian forests³⁷, restricting confidence in future projections of climate change over the region. Indeed, most of the dynamic global vegetation models (DGVMs) included in the TRENDY project (e.g., Friedlingstein et al.³⁸) and which are used to inform our best estimates of the global carbon budget assume that Amazon forests are represented by 1–2 discrete plant functional types (PFTs). For example, in the LPJ model³⁹ and the ORCHIDEE model⁴⁰ Amazon forest vegetation is described by a tropical evergreen PFT and a tropical deciduous PFT, while other vegetation models have an even more limited description of functional diversity (e.g., Galbraith et al.⁴¹). Such architectural restrictions mean that spatial variation in forest biomass storage and dynamics is poorly captured by many DGVMs⁴² and limit ability to capture variation in forest sensitivity to drought. However, there have been notable recent attempts to improve the description of functional diversity in DGVMs which replace prescribed trait values with more flexible trait values shaped by climate and competition (e.g. Thonicke et al. 2020⁴³). Such approaches present promising avenues for better representation of variation in forest sensitivity to climate in global models.

While our study documents spatial patterns and large-scale controls on forest sensitivity to drought in Amazonia, it does not allow for the determination of the specific mechanisms which underpin these differences. These may include variation across forests in ability to withstand negative xylem tensions under drought or belowground rooting properties. Elucidating these mechanisms is of high importance to enable more informed predictions of the impact of climate on this critically important biome, but is not yet possible due to the lack of Amazon basin scale databases of relevant plant traits. Thus while our study identifies patterns of varying climatic sensitivity across Amazon forests and the overarching controls of climate and soils, an understanding of the specific mechanisms will only be possible with new basin-wide products of plant functional properties.

Methods

Study area. This study focuses on forested areas with minimal human impacts within Amazonia. Amazonia was delineated using the geographical boundaries described by Feldpausch et al.⁴⁴ which is based on a combination of climate, hydrology, flora, fauna and biogeography criteria. These regions vary markedly in forest composition and dynamics and have been used extensively to evaluate how forest structure and function vary across different biogeographical regions^{42,44,45}. We restrict our analysis to Amazonian forests defined using the Intact Forest data product which maps unbroken expanses of natural ecosystems within the zone of current forest extent, having a minimum tree cover of 20%, and with no remotely detected signs of human activity⁴⁶. Savanna ecosystems as identified using the WWF Ecoregions⁴⁷ were excluded from the analysis to restrict our study to forest areas. As a final step, any forested pixels that experienced a fire in 2015 were identified using the MOD14A2 8-day fire product⁴⁸ and removed.

Overarching approach. We modelled 2015/16 ENSO-associated anomalies in photosynthetic activity over Amazonia as a function of variables representing the ENSO-associated climate anomalies, soil characteristics, and background climatology. The relative importance of each of these groups of variables and of the individual variables within these groups was then explored using multivariate regression analysis with final model selection based on Akaike's Information Criteria (AIC) and model stability analysis. The full model and explanation of variables are provided in the supplementary information (Supplementary Table 1).

SIF data. Photosynthetic activity was proxied using SIF retrieved at 09:30 hrs local time using the SIFTERv2 algorithm⁴⁹. The SIFTERv2 algorithm retrieves SIF from GOME-2A reflectance spectra in the 734–758 nm window, by examining the filling in of Fraunhofer lines relative to the depth of the Fraunhofer lines observed over the non-vegetated reference region of the Sahara, while accounting for the influence of the surface albedo and atmospheric transmission⁴⁹. The algorithm improves on previous versions of the SIFTER algorithm used by previous studies¹⁰ by explicitly attempting to correct for sensor degradation effects post 2013 (Supplementary Fig. 5) and by using narrower spectral windows that avoid oxygen absorption and are less sensitive to water vapour. The SIFTERv2 product corrects

for sensor degradation through analysis of changes in reflectance over the sites where reflectance is known to be stable⁴⁹. Data from this analysis was used to calculate degradation correction spectra for all seasons post July 2014, and these correction spectra were subsequently applied prior to the spectral retrieval to stabilise the observed declines. The corrected product removes any large-scale SIF trends over our study period (up to the end of 2016) and also reveals a rebound in SIF values in 2017 (Fig. 1). We note, however, that caution should be applied when using the product beyond the timeframe of this study as post-2017 SIF values appear to be associated with lower seasonal maxima and minima than values up to that point (Supplementary Fig. 5).

Daily SIF Retrievals from 2007 to 2017 from the SIFTERv2 algorithm⁵⁰ were resampled to a monthly mean $0.5^\circ \times 0.5^\circ$ gridded resolution using an inverse distance weighting algorithm implemented using the python library Pyresample⁵¹. Following the advice set out in the SIFTERv2 Algorithm Theoretical Basis Document⁵², pixel-level retrievals with QA values less than 0.6 were excluded from the study to ensure that only high-quality (low cloud fraction, small spectral residual) retrievals were used. QA values are calculated pixel wise from cloud fraction and spectral residual, pixels with high cloud fraction and high spectral residual will have a small QA value.

The monthly mean gridded data were then used to calculate a standardised SIF anomaly (Eq. 2):

$$\text{Standardised Anomaly} = \frac{X_t - \bar{X}}{\sigma} \quad (2)$$

where X_t represents the mean SIF value during the October to December 2015 period, \bar{X} represents the mean and σ the standard deviation of the baseline period (October to December) between 2007 and 2014 (excluding 2015). Information after the ENSO period was not included in the calculation of the baseline as evidence suggests that Amazonian forest dynamics following ENSO have changed significantly⁵³. Wigneron et al. 2020⁵³ for instance show that above-ground biomass (AGB) had not recovered by the end of 2017. Thus, we excluded post ENSO years in the calculation of the baseline as a precaution. October to December was chosen as the analysis period as this corresponded to the period of most negative SIF anomalies across all Amazon regions, as shown in previous studies that examined the SIF response to the 2015/2016 ENSO event^{10,54} and shown in Fig. 1.

The interpretation of changes in SIF as changes in productivity has been used by several studies^{10,23,55} including this one. However, the relationship is complicated, and the use of SIF as a proxy in this manner comes with a number sources of uncertainty and assumptions that must be taken into consideration when interpreting the results. Porcer-Castell et al.⁵⁶, summarised the key uncertainties surrounding interpreting SIF as productivity and we recommend the reader to read their work for a comprehensive summary. However, the key uncertainties relevant to this study include⁵⁶: 1. A lack of understanding of how alternative energy sinks e.g. photorespiration may help sustain electron transport during stress conditions when carbon assimilation and thus productivity is impaired resulting in a potential decoupling of SIF and productivity. 2. Uncertainty due to variation in species and leaf biochemistry, canopy architecture and the presence of non-photosynthetic material. 3. Uncertainty arising from the integration of SIF controls across space and time that may strengthen or disrupt the SIF-GPP relationship. While it is important to acknowledge these uncertainties when interpreting the results, we remain confident in our findings, as many studies^{57–60} examining SIF-GPP relationships to date find strong agreement in terms of variance explained, between SIF and GPP when using data collected from flux-towers, ground measured SIF, and remote sensing SIF products at spatio-temporal scales both finer and coarser than used in this study.

Climate anomalies associated with the ENSO. ENSO-associated climate anomalies were calculated as anomalies in mean monthly temperature, precipitation and Cumulative Water Deficit (CWD) using Eq. 1 where in this case X_t represents the mean temperature, precipitation or CWD value during the October to December 2015 period, \bar{X} represents the mean, and σ the standard deviation of the baseline period (October to December) between 2007 and 2014 (excluding 2015). Temperature data was retrieved from ERA5 monthly aggregates⁶¹, and precipitation data from TRMM 3B43 monthly precipitation product⁶². CWD was computed monthly as the difference between precipitation and potential evapotranspiration (PET)⁶³ (i.e., vegetation is assumed to experience stress when $PET > \text{precipitation}$), with deficits accumulated over all months where precipitation was inferior to PET and being reset to zero when precipitation exceeded PET. The evapotranspiration threshold was explored using two different methods, the first being a constant threshold set at 100 mm a month, based on mean water fluxes from tower networks and remote sensing products⁶⁴ and in line with many other studies on Amazon forests⁶⁵. However, we acknowledge that evapotranspiration can vary substantially across different Amazonian forest as studies have found that some regions have a monthly evapotranspiration closer to 150 mm⁶⁶. Thus, we also explored the implications of computing MCWD using other absolute thresholds. The conclusions of our analysis did not change for a range of evapotranspiration thresholds (Supplementary Fig. 2). The second method we tested, was using a satellite (MODIS) derived Potential Evapotranspiration⁴⁸ product. This product allowed us to calculate estimates of PET at a monthly timescale. Each month's PET average was subtracted from that month's rainfall to calculate the water deficit.

This was then accumulated over time to calculate MCWD resetting to zero if rainfall exceeded PET as before. This methodology arguably allows for a more realistic variation and estimation of PET than a simple threshold applied across all Amazonian forests. The results shown in this paper are based on this methodology.

Where required, climatic data were temporally and spatially resampled to match the resolution of the SIF data to ensure consistency of scale. After processing and applying quality filters, standardised anomalies were calculated for each ENSO-associated climate anomalies using Eq. 1.

Soil properties. Percentage sand and cation exchange capacity for different horizons from 0 to 30 cm depth were extracted from the SoilGrids dataset at a 1 km resolution⁶⁷. These were averaged over the entire 30 cm depth and resampled to match the SIF dataset spatial dimensions. Water table depth was retrieved from the water table depth map produced by Fan et al.²⁷, based on a data-model fusion approach. As with all other data layers, this product was spatially resampled to the resolution of the SIF data.

Soils grids are produced through interpolation from ground collected data accounting for a range of environmental covariates using machine learning algorithms. The quality of this product at any particular point, therefore, relies on number of points in the region, the distance from those points, and the scale of the analyses. The spatial coverage of the Amazon is good⁶⁷, especially when considering that this study is at a scale of 0.5×0.5 degrees with over 8000 soil profiles distributed across the study area. If this study was looking at finer scales, then issues of data validity may be of much higher concern, however at this scale it means that each of our pixels is covered by a good number of points, and thus is likely to be representative of the regional gradients in soil characteristics.

The Water table depth product used published by Fan et al.²⁷ interpolates globally from 1,603,781 observations of water table collected from government archives and published literature using a groundwater model forced by present-day climate, terrain and sea level²⁷. Observation density over the Amazon, is relatively low compared to other regions and this should be taken into account when interpreting water table depth. However, while water table depth at finer scales may differ from reality due to low data density, at the scale we are using, the data available should be sufficient to provide regional trends allowing us to test its importance. The Fan et al. product has been used extensively to evaluate the impacts of water availability on vegetation structure and function (e.g. Costa et al. 2022)⁶⁸.

Background climate variables. Background climate variables considered included mean annual precipitation and temperature, the interannual variability in mean annual precipitation and temperature and the seasonality of monthly precipitation and temperature. These variables were calculated using data from all years prior, and after ENSO, but excluding data from during the event itself (2015/16 data excluded). Temperature data was obtained from ERA5 and precipitation from TRMM 3B42, the same data used for the computation of ENSO-associated climate anomalies. The interannual variability was assessed by computing the coefficient of variation (CoV) across all years (except 2015), while the seasonality of precipitation was expressed as a seasonality index⁶⁹ using Eq. 3:

$$\overline{SI} = \frac{1}{\bar{R}} \sum_{n=1}^{12} \left| \bar{X}_n - \bar{R} \right| \quad (3)$$

where \bar{X}_n is the mean precipitation of month n , and \bar{R} is the mean annual precipitation. Seasonality in temperature was calculated as the average annual CoV of temperature. All data processing was performed using Google Earth Engine⁷⁰.

Statistical analysis. Explanatory variables were split into three overarching groups representing ENSO-associated climate anomalies, (temperature, precipitation, and CWD anomalies), soil characteristics (percentage sand, cation exchange capacity and water table depth) and background climatology (mean annual precipitation/temperature, interannual variability in precipitation/temperature and seasonality of precipitation/temperature). We considered both linear and quadratic terms for temperature anomaly to better represent its non-linear relationship with productivity, whereas all other variables were included as linear terms only. The full model and predictor variable description are provided in Supplementary Table 1. Model fit was assessed using standard model diagnostics in R, including calculating of model R^2 , QQ plots, leverage plots, plots for heteroscedasticity and a plot of fitted vs observed values (Supplementary Fig. 4).

Variable selection for the final model was undertaken using a backwards elimination algorithm based on AIC. During a single step variables are removed one at a time from the model and the change in AIC calculated. The variable which resulted in the greatest decrease in AIC was then eliminated. This process was repeated until the elimination of any variable results in a decrease in AIC of less than 2 producing the final model for interpretation. To remove confounding effects due to correlation between variables, variance inflation factors (VIF) were calculated for all variables before backward elimination was conducted and all variables with VIF greater than 10, indicating likely multicollinearity, were removed. K fold cross-validation was performed ($k = 10$) to check for overfitting. Root mean squared error of the final selected model was calculated as 0.862, and the average k -fold validation was 0.866, the similarity indicating that the selected model does not exhibit significant overfitting.

Model stability was investigated using a bootstrapping approach⁷¹ to quantify the extent to which our final model was stable to mild to moderate perturbation, and thus to what extent we can rely on the final model for inference. The underlying dataset was bootstrapped ($n = 1000$), and backward elimination used to produce a final model as outlined previously. Mean, standard deviation and 2.5/97.5 quantiles were then calculated from the bootstrapped population. Variables for which the 95 quantiles crossed zero were excluded from analysis as the direction of their relationship with SIF anomaly could not be reliably inferred.

Variable importance was assessed at two levels: (1) at a group level by calculating the change in final model R^2 when either ENSO-associated climate anomalies, soils or background climatology groups were eliminated and (2) at the level of the individual variable through direct comparison of scaled regression coefficients in the final model.

All statistical analysis was conducted using R version 4.0.0. Data visualisation was performed in R using the ggplot2 package⁷² and QGIS⁷³.

Data availability

All data made available through Google Earth Engine require the creation of a Google Earth Engine account <https://earthengine.google.com/> The daily level 2 SIF data are publicly available at https://www.temis.nl/surface/sif/sif_daily_gome2a.php, the Temis team request that authors send them a copy of any publications made using their data. A monthly averaged 0.5×0.5 gridded product created by the authors for this study can be found at <https://code.earthengine.google.com/?asset=users/MaxFancourt/updatedSIFTERID>. TRMM 3B43: Monthly Precipitation Estimates was used to calculate precipitation anomalies, mean annual precipitation, precipitation seasonality, variation in precipitation and MCWD is publicly available. This data is publicly available at https://developers.google.com/earth-engine/datasets/catalog/TRMM_3B43V7 ERA5 Monthly Aggregates - Latest Climate Reanalysis Produced by ECMWF/Copernicus Climate Change Service was used to calculate temperature anomalies, mean annual temperature, and variation in temperature. This data is publicly available at https://developers.google.com/earth-engine/datasets/catalog/ECMWF_ERA5_MONTHLY MOD16A2.006: Terra Net Evapotranspiration 8-Day Global 500 m was used to calculate potential evapotranspiration as part of the calculation of MCWD. The data is publicly available at https://developers.google.com/earth-engine/datasets/catalog/MODIS_006_MOD16A2 Cation Exchange Capacity, as well as soil clay and sand content was obtained from SoilGrids is publicly available at <https://www.isric.org/explore/soilgrids> Water table depth was provided by Fan et al.²⁷ and is available upon request of Fan et al, contact details in their paper. All anomalies, and explanatory derived variables are available via the Google Earth Engine Code Link in the code availability section.

Code availability

The remote sensing portion of this analysis was conducted in Google Earth Engine, the code for which is publicly available via the links below upon the creation of a Google Earth Engine account. The SIF and Climate Anomalies data was produced using Google Earth Engine, the code to reproduce this data: <https://code.earthengine.google.com/9813c6ed96a952f8e0380cc19d1b594a> The explanatory variables (mean annual precipitation, mean annual temperature, inter and intra annual variation in precipitation and temperature, seasonality in precipitation and variance in temperature and precipitation are available using the following link: <https://code.earthengine.google.com/619ee4021025e179d2dc4b1e0f0e1753> The statistical analysis to conduct this analysis, was conducted in R and is available along with the data to replicate this analysis for download from <https://zenodo.org/badge/latestdoi/51423121174> The code and data to replicate all figures in the main text and supplementary information is available from <https://zenodo.org/badge/latestdoi/51423121174>.

Received: 16 July 2021; Accepted: 11 August 2022;

Published online: 16 September 2022

References

- Costanza, R. et al. Changes in the global value of ecosystem services. *Glob. Environ. Change* **26**, 152–158 (2014).
- Mittermeier, R. A. et al. Wilderness and biodiversity conservation. *Proc. Natl. Acad. Sci. USA* **100**, 10309–10313 (2003).
- Dirzo, R. & Raven, P. H. Global state of biodiversity and loss. *Annu. Rev. Env. Resour.* **28**, 137–167 (2003).
- Marengo, J. A. et al. Changes in climate and land use over the amazon region: current and future variability and trends. *Front. Earth Sci.* **6**, 1–21 (2018).
- Anderson-Teixeira, K. J. et al. Climate-regulation services of natural and agricultural ecoregions of the Americas. *Nat. Clim. Change* **2**, 177–181 (2012).

6. Marengo, J. A. et al. The drought of Amazonia in 2005. *J. Clim.* **21**, 495–516 (2008).
7. Lewis, S. L., Brando, P. M., Phillips, O. L., Van Der Heijden, G. M. F. & Nepstad, D. The 2010 Amazon drought. *Science* **331**, 554 (2011).
8. Jiménez-Muñoz, J. C. et al. Record-breaking warming and extreme drought in the Amazon rainforest during the course of El Niño 2015–2016. *Sci. Rep.* **6**, 33130 (2016).
9. Phillips, O. L. et al. Drought sensitivity of the Amazon rainforest. *Science* **323**, 1344–1347 (2009).
10. Koren, G. et al. Widespread reduction in sun-induced fluorescence from the Amazon during the 2015/2016 El Niño. *Philos. Trans. R. Soc. Lond. B Biol. Sci.* **373**, 20170408 (2018).
11. Feldpausch, T. R. et al. Amazon forest response to repeated droughts. *Glob. Biogeochem. Cycles* **30**, 964–982 (2016).
12. Sousa, T. R. et al. Palms and trees resist extreme drought in Amazon forests with shallow water tables. *J. Ecol.* **108**, 2070–2082 (2020).
13. Barros, F. et al. Hydraulic traits explain differential responses of Amazonian forests to the 2015 El Niño-induced drought. *New Phytol.* **223**, 1253–1266 (2019).
14. Magney, T. S. et al. Mechanistic evidence for tracking the seasonality of photosynthesis with solar-induced fluorescence. *Proc. Natl Acad. Sci. USA* <https://doi.org/10.1073/pnas.1900278116> (2019).
15. Ciemer, C. et al. Higher resilience to climatic disturbances in tropical vegetation exposed to more variable rainfall. *Nat. Geosci.* **12**, 174–179 (2019).
16. Gloor, E. et al. Tropical land carbon cycle responses to 2015/16 El Niño as recorded by atmospheric greenhouse gas and remote sensing data. *Philos. Trans. R. Soc. B* **373**, 20170302 (2018).
17. Jiménez-Muñoz, J. C., Sobrino, J. A., Mattar, C. & Malhi, Y. Spatial and temporal patterns of the recent warming of the Amazon forest. *J. Geophys. Res. Atmos.* **118**, 5204–5215 (2013).
18. Choat, B. et al. Global convergence in the vulnerability of forests to drought. *Nature* **491**, 752–755 (2012).
19. Esquivel-Muelbert, A. et al. Seasonal drought limits tree species across the Neotropics. *Ecography* **60**, 12 (2016).
20. Fisher, R. A., Williams, M., de Lourdes Ruivo, M., de Costa, A. L. & Meir, P. Evaluating climatic and soil water controls on evapotranspiration at two Amazonian rainforest sites. *Agric. For. Meteorol.* **148**, 850–861 (2008).
21. Marthews, T. R. et al. High-resolution hydraulic parameter maps for surface soils in tropical South America. *Geosci. Model Dev.* **7**, 711–723 (2014).
22. Esteban, E. J. L., Castilho, C. V., Melgaço, K. L. & Costa, F. R. C. The other side of droughts: wet extremes and topography as buffers of negative drought effects in an Amazonian forest. *New Phytol.* **229**, 1995–2006 (2021).
23. Castro, A. O. et al. OCO-2 solar-induced chlorophyll fluorescence variability across ecoregions of the Amazon basin and the extreme drought effects of El Niño (2015–2016). *Remote Sens.* **12**, 1202 (2020).
24. Sullivan, M. J. P. et al. Long-term thermal sensitivity of Earth's tropical forests. *Science* **368**, 869–874 (2020).
25. Sombroek, W. Spatial and temporal patterns of Amazon rainfall. *Ambio* **30**, 388–396 (2001).
26. Quesada, C. A. et al. Basin-wide variations in Amazon forest structure and function are mediated by both soils and climate. *Biogeosciences* **9**, 2203–2246 (2012).
27. Fan, Y., Li, H. & Miguez-Macho, G. Global patterns of groundwater table depth. *Science* **339**, 940–943 (2013).
28. Joetzer, E., Douville, H., Delire, C. & Ciais, P. Present-day and future Amazonian precipitation in global climate models: CMIP5 versus CMIP3. *Clim. Dyn.* **41**, 2921–2936 (2013).
29. Schiatti, J. et al. Vertical distance from drainage drives floristic composition changes in an Amazonian rainforest. *Plant. Ecol. Divers.* **7**, 241–253 (2014).
30. Oliveira, R. S. et al. Embolism resistance drives the distribution of Amazonian rainforest tree species along hydro-topographic gradients. *New Phytol.* **221**, 1457–1465 (2018).
31. Fyllas, N. M. et al. Basin-wide variations in foliar properties of Amazonian forest: phylogeny, soils and climate. *Biogeosciences* **6**, 2677–2708 (2009).
32. Sterck, F., Markesteijn, L., Schieving, F. & Poorter, L. Functional traits determine trade-offs and niches in a tropical forest community. *PNAS* **108**, 20627–20632 (2011).
33. Oliveira, R. S. et al. Linking plant hydraulics and the fast–slow continuum to understand resilience to drought in tropical ecosystems. *New Phytol.* **230**, 904–923 (2021).
34. Guillemot, J. et al. Small and slow is safe: On the drought tolerance of tropical tree species. *Glob. Chang. Biol.* **28**, 2622–2638 (2022).
35. DeSoto, L. et al. Low growth resilience to drought is related to future mortality risk in trees. *Nat. Commun.* **11**, 545 (2020).
36. Rowland, L. et al. Death from drought in tropical forests is triggered by hydraulics not carbon starvation. *Nature* **528**, 119–122 (2015).
37. de Almeida Castanho, A. D. et al. Changing Amazon biomass and the role of atmospheric CO₂ concentration, climate, and land use. *Glob. Biogeochem. Cycles* **30**, 18–39 (2016).
38. Friedlingstein, P. et al. Global carbon budget 2020. *Earth Syst. Sci. Data* **12**, 3269–3340 (2020).
39. Sitch, S. et al. Evaluation of ecosystem dynamics, plant geography and terrestrial carbon cycling in the LPJ dynamic global vegetation model. *Glob. Chang. Biol.* **9**, 161–185 (2003).
40. Lathière, J. et al. Impact of climate variability and land use changes on global biogenic volatile organic compound emissions. *Atmos. Chem. Phys.* **6**, 2129–2146 (2006).
41. Galbraith, D. et al. Multiple mechanisms of Amazonian forest biomass losses in three dynamic global vegetation models under climate change. *New Phytol.* **187**, 647–65 (2010).
42. Johnson, M. O. et al. Variation in stem mortality rates determines patterns of above-ground biomass in Amazonian forests: implications for dynamic global vegetation models. *Glob. Chang. Biol.* **22**, 3996–4013 (2016).
43. Thonicke, K. et al. Simulating functional diversity of European natural forests along climatic gradients. *J. Biogeogr.* **47**, 1069–1085 (2020).
44. Feldpausch, T. R. et al. Height-diameter allometry of tropical forest trees. *Biogeosciences* **8**, 1081–1106 (2011).
45. Feldpausch, T. R. et al. Tree height integrated into pantropical forest biomass estimates. *Biogeosciences* **9**, 3381–3403 (2012).
46. Potapov, P. et al. The last frontiers of wilderness: tracking loss of intact forest landscapes from 2000 to 2013. *Sci. Adv.* **3**, 1–14 (2017).
47. Olson, D. M. et al. Terrestrial ecoregions of the world: a new map of life on Earth. *BioScience* **51**, 933–938 (2001).
48. Running, Steve, Mu, Qiaozhen & Zhao, Maosheng. MOD16A2 MODIS/Terra net evapotranspiration 8-day L4 global 500m. <https://doi.org/10.5067/MODIS/MOD16A2.006> (2017).
49. van Schaik, E. et al. Improved SIFTER v2 algorithm for long-term GOME-2A satellite retrievals of fluorescence with a correction for instrument degradation. <https://doi.org/10.5194/amt-2019-384> (2020).
50. Kooreman, M. L. et al. GOME-2A SIFTER v2 (2007–2018) [Data set]. *SIFTER sun-induced vegetation fluorescence data from GOME-2A (Version 2.0) [Data set]*. Royal Netherlands Meteorological Institute (KNMI). <https://doi.org/10.21944/gome2a-sifter-v2-sun-induced-fluorescence>.
51. Hoese, D. et al. *pytroll/pyresample: Version 1.23.0*. Zenodo, <https://doi.org/10.5281/zenodo.6375741> (2022).
52. Kooreman, M., Tuinder, O., Boersma, K. F. & van Schaik, E. Algorithm Theoretical Basis Document for the GOME-2 NRT, Offline and Data Record Sun-Induced Fluorescence Products. (2019).
53. Wigneron, J.-P. et al. Tropical forests did not recover from the strong 2015–2016 El Niño event. *Sci. Adv.* **6**, eaay4603 (2020).
54. Gatti, L. V. et al. Drought sensitivity of Amazonian carbon balance revealed by atmospheric measurements. *Nature* **506**, 76–80 (2014).
55. Doughty, R. et al. TROPOMI reveals dry-season increase of solar-induced chlorophyll fluorescence in the Amazon forest. *Proc. Natl. Acad. Sci. USA* **116**, 22393–22398 (2019).
56. Porcar-Castell, A. et al. Chlorophyll a fluorescence illuminates a path connecting plant molecular biology to Earth-system science. *Nat. Plants* **7**, 998–1009 (2021).
57. Sun, Y. et al. OCO-2 advances photosynthesis observation from space via solar-induced chlorophyll fluorescence. *Science* **358**, eaam5747 (2017).
58. Wood, J. D. et al. Multiscale analyses of solar-induced fluorescence and gross primary production. *Geophys. Res. Lett.* **44**, 533–541 (2017).
59. Verma, M. et al. Effect of environmental conditions on the relationship between solar-induced fluorescence and gross primary productivity at an OzFlux grassland site. *J. Geophys. Res. Biogeosci.* **122**, 716–733 (2017).
60. Parazoo, N. C. et al. Terrestrial gross primary production inferred from satellite fluorescence and vegetation models. *Glob. Chang. Biol.* **20**, 3103–3121 (2014).
61. Copernicus Climate Change Service (C3S). ERA5: Fifth generation of ECMWF atmospheric reanalyses of the global climate. <https://cds.climate.copernicus.eu/cdsapp#!/home> (2017).
62. Goddard Earth Sciences Data and Information Services Center (GES DISC). Tropical Rainfall Measuring Mission (TRMM) - TRMM (TMPA/3B43) Rainfall Estimate L3 1 month 0.25 degree x 0.25 degree V7. <https://doi.org/10.5067/TRMM/TMPA/MONTH/7> (2011).
63. Aragão, L. E. O. C. et al. Spatial patterns and fire response of recent Amazonian droughts. *Geophys. Res. Lett.* **34** (2007).
64. Paca, V. H. et al. The spatial variability of actual evapotranspiration across the Amazon River Basin based on remote sensing products validated with flux towers. *Ecol. Process.* **8**, 6 (2019).
65. Phillips, O. L. et al. Drought–mortality relationships for tropical forests. *New Phytol.* **187**, 631–646 (2010).
66. Maeda, E. E. et al. Evapotranspiration seasonality across the Amazon Basin. *Earth Syst. Dyn.* **8**, 439–454 (2017).
67. Hengl, T. et al. SoilGrids250m: Global gridded soil information based on machine learning. *PLoS One* **12**, e0169748 (2017).
68. Costa, F. R. C., Schiatti, J., Stark, S. C. & Smith, M. N. The other side of tropical forest drought: do shallow water table regions of Amazonia act as

- large-scale hydrological refugia from drought? *New Phytol.* <https://nph.onlinelibrary.wiley.com/doi/10.1111/nph.17914> .
69. Walsh, R. P. D. & Lawler, D. M. Rainfall seasonality: description, spatial patterns and change through time. *Weather* **36**, 201–208 (1981).
 70. Gorelick, N. et al. Google Earth Engine: Planetary-scale geospatial analysis for everyone. *Remote Sens. Environ.* <https://doi.org/10.1016/j.rse.2017.06.031> (2017).
 71. Heinze, G., Wallisch, C. & Dunkler, D. Variable selection – a review and recommendations for the practicing statistician. *Biom. J.* **60**, 431–449 (2018).
 72. Wickham, H. *ggplot2: Elegant Graphics for Data Analysis* (Springer-Verlag New York, 2016).
 73. QGIS.org. *QGIS Geographic Information System* (QGIS Association, 2022).
 74. Fancourt, M. Repository for Code, Data and Figures. <https://zenodo.org/badge/latestdoi/10.5281/zenodo.514231211> (2022).

Acknowledgements

We would like to acknowledge EUMETSAT for the GOME-2 and TRMM data, www.temis.nl for the SIFTER v2 data, the Copernicus Climate Change Service for ERA5 data, the Soil grids team for soils data, Global Forest Watch for the Intact Forests data, Michelle Johnson for providing the shapefile for the Amazon biogeographical regions and Ying Fan, Haibin Li and Gonzalo Miguez-Macho for the water table depth dataset. MF was funded by a NERC DTP studentship (NE/L002574/1). DG acknowledges support from two NERC awards (ARBOLES - NE/S011811/1 and TREMOR - NE/N004655/1).

Author contributions

M.F, D.G and G.Z conceived the study. M.F conducted the analysis. M.F, D.G and G.Z contributed to the interpretation of the results and development of the study. K.F.B provided technical information and assistance with the SIFTERv2 data product. J.T and Y.W provided technical information and assistance with interpreting the results and their impacts on forests. All authors contributed to the writing and revision of the manuscript.

Competing interests

The authors declare no competing interests.

Additional information

Supplementary information The online version contains supplementary material available at <https://doi.org/10.1038/s43247-022-00533-3>.

Correspondence and requests for materials should be addressed to Max Fancourt.

Peer review information *Communications Earth & Environment* thanks Gregory Duveiller and the other, anonymous, reviewer(s) for their contribution to the peer review of this work. Primary Handling Editors: Regina Rodrigues and Clare Davis. Peer reviewer reports are available.

Reprints and permission information is available at <http://www.nature.com/reprints>

Publisher's note Springer Nature remains neutral with regard to jurisdictional claims in published maps and institutional affiliations.



Open Access This article is licensed under a Creative Commons Attribution 4.0 International License, which permits use, sharing, adaptation, distribution and reproduction in any medium or format, as long as you give appropriate credit to the original author(s) and the source, provide a link to the Creative Commons license, and indicate if changes were made. The images or other third party material in this article are included in the article's Creative Commons license, unless indicated otherwise in a credit line to the material. If material is not included in the article's Creative Commons license and your intended use is not permitted by statutory regulation or exceeds the permitted use, you will need to obtain permission directly from the copyright holder. To view a copy of this license, visit <http://creativecommons.org/licenses/by/4.0/>.

© The Author(s) 2022